A critical role for NMDA receptors in parvalbumin interneurons for gamma rhythm induction and behavior

Marie Carlen, Konstantinos Meletis, Joshua Siegle, Jessica Cardin, Kensuke Futai, Dorea Vierling-Claassen, Charlotta Ruehlmann, Stephanie R Jones, Karl Deisseroth, Morgan Sheng, et al.

A critical role for NMDA receptors in parvalbumin interneurons for gamma rhythm induction and behavior

Marie Carlén, PhD[1,2*], Konstantinos Meletis, PhD[1,2*], Joshua H. Siegle[3], Jessica A. Cardin. PhD[3,4], Kensuke Futai, PhD[1], Dorea Vierling-Claassen, PhD[3,4], Charlotta Rühlmann[1], Stephanie R. Jones, PhD[5], Karl Deisseroth, M.D., PhD[6], Morgan Sheng, M.B.B.S., PhD[1], Christopher I. Moore, PhD[3] and Li-Huei Tsai, PhD[1,7,8]

[1]Picower Institute for Learning and Memory, Department of Brain and Cognitive Sciences, MIT, Cambridge, MA. [2]Department of Neuroscience, Karolinska Institutet, Stockholm, Sweden, [3]McGovern Institute for Brain Research and Department of Brain and Cognitive Sciences, MIT, Cambridge MA. [4]Department of Neuroscience, University of Pennsylvania, Philadelphia, PA. [5]Athinoula A. Martinos Center for Biomedical Imaging, Massachusetts General Hospital, Harvard Medical School, Charlestown, MA. [6]Department of Bioengineering, Stanford University, Stanford, CA. [7]Stanley Center for Psychiatric Research, Broad Institute of Harvard and Massachusetts Institute of Technology, Cambridge MA. [8]Howard Hughes Medical Institute, Cambridge, MA.

Running title: NMDAR in PV interneurons for gamma and behavior

*) These authors contributed equally

Correspondence:

Dr M Carlén
Department of Neuroscience
Karolinska Institutet
Retzius väg 8
171 77 Stockholm, Sweden
Phone: +46-70-459 55 77

Fax: +46-8-333 864
Email: marie.carlen@ki.se

or

Dr C I Moore
McGovern Institute for Brain Research
Massachusetts Institute of Technology
77 Massachusetts Avenue
Cambridge, MA 02139, USA
Phone: +1-617-324-3769
Fax: +1-617-452-4119
Email: cim@mit.edu

Or

Dr L-H Tsai
Picower Institute for Leaning and Memory
Massachusetts Institute of Technology
77 Massachusetts Avenue
Cambride, MA 02139, USA
Phone: +1-617-324-1658
Fax: +1-617-324-1657
Email: lhtsai@mit.edu

Abstract

Synchronous recruitment of fast-spiking parvalbumin interneurons generates gamma oscillations, rhythms that emerge during performance of cognitive tasks. Administration of NMDA receptor antagonists alters gamma rhythms, and can induce cognitive as well as psychosis-like symptoms in humans. The disruption of NMDA receptor signaling specifically in fast-spiking parvalbumin interneurons is therefore hypothesized to give rise to neural network dysfunction that could underlie these symptoms. To address the connection between NMDA receptor activity, fast-spiking parvalbumin interneurons, gamma oscillations and behavior, we generated mice lacking NMDA receptor neurotransmission only in parvalbumin

cells (PV-Cre/NR1f/f mice). Here we show that mutant mice exhibit enhanced baseline cortical gamma rhythms, impaired gamma rhythm induction after optogenetic drive of parvalbumin interneurons and reduced sensitivity to the effects of NMDA receptor antagonists on gamma oscillations and stereotypies. Mutant mice show largely normal behaviors except for selective cognitive impairments, including deficits in habituation, working memory and associative learning. Our results provide evidence for the critical role of NMDA receptors in parvalbumin interneurons for expression of normal gamma rhythms and specific cognitive behaviors.

Keywords: parvalbumin; interneurons; gamma; NMDAR; optogenetics; oscillations

Introduction

Fast-spiking (FS) parvalbumin (PV) interneurons are GABAergic cells that express the Ca^{2+}-binding protein parvalbumin and receive N-methyl-D-aspartate (NMDA)-dependent excitatory input from pyramidal cells (1). FS-PV interneurons regulate the activity of neural networks through gamma-aminobutyric acid (GABA)-ergic inhibition of local excitatory neurons, and synchronous activity of FS interneurons generates gamma oscillations (30-80 Hz) (2-6). Normal gamma oscillations are correlated with performance of a variety of cognitive tasks, including the allocation of attention and working memory (7). Consistent with the importance of gamma oscillations, and with the more general requirement of appropriate inhibition in neural circuits, FS-PV interneurons have been proposed to underlie the cognitive disturbances associated with psychiatric disorders (8).

The NMDA receptor (NMDAR) has also been directly implicated in the emergence of gamma rhythms, as NMDAR antagonists can disrupt (9) or potentiate (10), gamma rhythms in slices and *in vivo* (11-15). This aspect of the glutamatergic system is also implicated in cognitive disturbances by the psychotomimetic effects of NMDAR antagonists (16, 17), which recapitulate core features of schizophrenia, most notably cognitive deficits in planning, attention, learning and memory (18, 19). Further, schizophrenic patients display aberrant induction of gamma oscillations during cognitive tasks (7, 20, 21).

These intersecting lines of evidence strongly implicate PV interneurons and NMDAR in the expression of gamma rhythms in normal cognitive function and in disease. To directly test the impact of NMDAR function in PV interneurons on gamma

oscillation expression and behavior, we generated mice lacking NMDAR only in PV neurons. We then probed the resting-state expression of gamma oscillations, and their induction through optogenetic and pharmacological means. We also measured a variety of behaviors ranging from sensorimotor gating to cognitive dimensions such as working memory. We found that selective deletion of NMDAR from PV cells leads to an enhanced resting-state expression of gamma oscillations and a deficit in gamma induction. Further, we found a selective pattern of behavioral disturbance that spares several metrics but impairs expression of habituation, working memory and other learning indices. These data strongly support the role of NMDAR on PV cells in normal gamma functionality in the *in vivo* mammalian neocortex, and indicate a specific role for it in selective aspects of learning and memory.

Materials and Methods

Animals

All procedures were conducted in accordance with the National Institutes of Health guidelines and with the approval of the Committee on Animal Care at MIT. We generated PV-Cre/NR1f/f mice by crossing of PV-Cre mice (22) with mice carrying "floxed" NR1 alleles (23). In awake electrophysiology and behavior tests male PV-Cre/NR1f/f mice and littermate male controls (NR1f/f) were used. For slice electrophysiology and optogenetic experiments in anesthetized animals age-matched male PV-Cre mice were used as controls.

Immunohistochemistry

Free floating sections (30 μm) were prepared and immunostained (4). The following primary antibodies were used: Parvalbumin PVG-214 (Swant; 1:2000), EYFP (GFP-1020 Aves; 1:500). Antibody staining was revealed using species-specific fluorophore-conjugated secondary antibodies (Cy5 from Jackson, Alexa 488 from Molecular Probes).

Quantification

Cre recombination was quantified in PV-Cre mice crossed to the R26R-EYFP Cre reporter mouse line (24). Free-floating sections stained with antibodies against PV and EYFP were used. For quantification of recombination in S1, every PV cell was counted and scored for co-labeling with EYFP in 1190.30 x 1190.30 x 30 μm images including all six cortical layers. For quantification of recombination in hippocampus every PV cell in dentate gyrus, CA1, CA2 and CA3 was counted and scored for co-labeling with EYFP.

For quantification of the number and distribution of PV cells in S1 in NR1f/f and PV-Cre/NR1f/f mice and every PV cell was counted as describe above and assigned to layers 2/3 or 4-6 based on its position in relation to the layer 4 barrels.

Slice electrophysiology

AAV DIO ChR2-mCherry (4) was injected into hippocampus of 5-7 week old PV-Cre and PV-Cre/NR1f/f mice. 7-10 days after viral transduction transverse hippocampal slices (400 mm thickness) were prepared as described (25, 26). The tungsten bipolar electrode (FHC) was placed in the stratum radiatum or oriens and the Schaffer collateral/commissural fibers were stimulated at 0.1 Hz. Picrotoxin (0.15 mM, Sigma)

was dissolved in aCSF to block $GABA_A$ receptor-mediated synaptic transmission for whole-cell patch clamp recordings. AMPA receptor-mediated EPSCs were recorded at -70 mV, and NMDA receptor-mediated EPSCs were recorded at +40 mV with the same stimulus strength in the presence of NBQX (0.005 mM, Tocris).

Anesthetized electrophysiology

AAV DIO ChR2-mCherry was injected into barrel cortex of adult (8-12 w old) PV-Cre or PV-Cre/NR1f/f mice as described earlier (4). Electrophysiological *in vivo* recordings were performed 1-3 w after viral injections. Extracellular single-unit and local field potential recordings were made with tetrodes or stereotrodes. Stimulus control and data acquisition was performed using software custom written in LabView (National Instruments, Austin TX) and Matlab (The Mathworks, Natick MA) by Ulf Knoblich.

Light stimulation was generated by a 473 nm laser and light pulses were given via a 200 mm diameter, unjacketed optical fiber at the cortical surface 75-200 mm from the recording electrodes.

Unit and local field potential analysis used software custom written in Igor Pro (Wavemetrics, Portland OR) by J.A.C. Spontaneous anesthetized LFP measurements were made during periods with no light stimulation. For each light stimulation frequency, we measured relative power (27-29) in an 8 Hz band centered on that frequency. Relative power was used to account for differences in LFP amplitude between recording sites and between electrodes. Relative power was calculated by measuring the ratio of power within the band of interest to total power (1-100 Hz) in the power spectrum of the unfiltered LFP (for details see Supplementary Information; Extended Materials and

Methods). For each recording site, we measured power from 10-30 LFP traces under each condition. Example power spectra are population averages. We also measured the power ratio:

$$P_{light}/ P_{baseline}$$

where P_{light} is the relative power in a frequency band in the presence of light stimulation and $P_{baseline}$ is the power in that band in the absence of light stimulation.

Spike waveforms of regular spiking (RS) and fast spiking (FS) cells were characterized. In each case, FS measurements were made from cells expressing ChR2 and driven by light pulses and RS measurements were made from non-driven, spontaneously active cells. Statistical significance was assessed with the Mann-Whitney test. All numbers are given as mean ± SEM, except where otherwise noted.

Awake electrophysiology

Eight NR1f/f control and eight PV-Cre/NR1f/f mice (8-10w) were used for awake electrophysiology. Teflon-coated tungsten electrodes (impedance of 100 kΩ) were implanted: two electrodes were placed bilaterally in primary somatosensory (barrel) cortices 1.5 mm posterior to bregma and 3.5 mm from the midline. In each hemisphere, a signal electrode was implanted 0.5 mm below the cortical surface and a reference electrode was implanted 1.75 mm below the cortical surface. A stainless steel screw over right posterior parietal cortex served as ground. Recording sessions took place in an empty box to which animals had not been previously exposed. After a 5-10 min habituation period, 20 min of baseline data were recorded for each animal. After the baseline period, four NR1f/f control and four PV-Cre/NR1f/f mice were injected

intraperitoneally with 0.5 mg/kg of MK-801 and four NR1f/f control and four PV-Cre/NR1f/f mice were injected intraperitoneally with saline and another 40 min of data were recorded. The behavioral state of all animals was scored by an observer blind to the genotype, and the sessions for ten of the animals were monitored with a video camera. All analysis was performed offline in Matlab. Normalized relative power indicates power normalized by both total power and by relative power during the baseline period, to highlight pre/post changes. Power change is the logarithm of the normalized relative power, which facilitates comparisons across frequency bands. Statistical significance was assessed with the Mann-Whitney test (between-group comparisons) and the Wilcoxon signed-rank test (within-group comparisons).

Mouse behavior

All behavioral tests were performed blind for the genotype of the mice. Male PV-Cre/NR1f/f mice and littermate male controls (NR1f/f) were used for all behavioral tests. Behavioral parameters were analyzed by *t* tests for the two genotypes, except for otherwise noted, and corrected for multiple comparisons. $P < 0.05$ was considered significant. All results are presented as mean ± SEM.

Open field analysis

Activity in a novel open field was measured in monitors with sets of 16 light beams arrays. During 60 min the hardware detected beams broken by the animal, with the software determining the location and activity of the animal. For the pharmacological treatment, one set of mice was first monitored in the open field for 30 min. Directly

thereafter MK-801 (M107; Sigma) (0.2 or 0.3 mg/kg) was injected intraperitoneally and the mice were monitored for additionally 60 min, in the same boxes as before.

Acoustic startle and prepulse inhibition

For testing of sensorimotor gating, startle response and prepulse inhibition (PPI) were determined using the Startle Monitor System (SM100; Hamilton Kinder). The animals were habituated to the experimental equipment for two days. Day three, the PPI testing day, each animal was exposed to 65 dB ambient noise for 5 min followed by the testing session. The PPI paradigm consisted of trials with presentation of a startle stimulus alone and trials where a prepulse of different preceded the startle stimulus by 100 ms. Trials were presented in blocks, with each block consisting of one startle stimulus alone trial, each of the prepulse-pulse stimulus trials, and a no stimulus trial, in a fixed pseudo randomized order. A total of six blocks were presented in a session and corresponding responses were averaged for each mouse and trial separately.

Habituation

Habituation of the startle reflex was assessed by comparing the mean startle amplitude of four pulses of a 120 dB white noise stimulus presented at the beginning and the end of the startle session using the equation [100-([mean startle block 2/ mean startle block 1) x100)].

T-maze test

For testing of working memory, a modified T-maze, the discrete paired-trial variable-delay alternation task, was used (30).

Contextual and cued fear conditioning

Context-dependent fear conditioning: The animals were placed in a novel conditioning chamber for 3 min where they were exposed to a foot shock. 24 h later, animals were returned to the same chamber and contextual memory was assessed as freezing during a 3 min test period. Tone-dependent (cued) fear conditioning: The animals were placed in the conditioning chamber for 3 min after which a 20 s tone (auditory cue) followed which co-terminated with a foot shock. 24 h later, animals were returned and cued fear learning was assessed. Before placement of the animals in the conditioning chamber, the environment in the chamber had been changed (visual, tactile and olfactory cues) to present the animals with a new context for the test.

Water Maze

The spatial reference task was a water maze task performed in a circular tank (diameter 1.8 m) filled with opaque water. A fixed platform (10 cm diameter) was hidden below the water's surface in the centre of the target quadrant. After training for several days, the platform was removed (probe trial). Reversal training started the day after the probe trial, followed by a probe trial for the new target quadrant.

Results

Genetic ablation of NMDAR signaling in parvalbumin interneurons

Previous mouse models of NMDAR hypofunction have targeted all neuronal classes, resulting in severe behavioral abnormalities (31, 32). To directly address the function of NMDAR specifically in PV interneurons in network function and cognitive behavior, we created mice lacking the NMDAR subunit NR1 only in PV expressing cells. Mice with Cre recombinase expression in PV cells (PV-Cre mice) (22) were crossed with mice carrying floxed alleles of the NR1 subunit (NR1f/f mice) (23).

Characterization of PV-Cre/NR1f/f mice

PV-Cre/NR1f/f mice were viable, developed normally and did not exhibit growth abnormalities or other gross anatomical changes (data not shown). Cre-dependent recombination from the PV locus was specific to PV expressing cells and followed the postnatal onset of PV expression (33) (Figure 1a). PV-Cre driven recombination in somatosensory cortex and hippocampus was detected at postnatal day 13 (P13) with increased recombination at 29 days (P29) and almost complete recombination at 8 weeks (Figure 1a, Supplementary Figure 1). Whole-cell recordings in hippocampal slices *in vitro* confirmed the functional loss of NMDAR currents in PV cells in PV-Cre/NR1f/f mice (5 cells in 4 PV-Cre/NR1f/f mice, 7 cells in 5 in control mice, $P = 0.03$, unpaired t-test; Figure 1b and c). We found the cortical architecture (layers and barrels in somatosensory cortex), migration and differentiation of PV interneurons to be normal in PV-Cre/NR1f/f mice (Figure 1d, e; $P = 0.65$ for layers 2/3 and $P = 0.53$ for layers 4-6, 2-tailed unpaired t-test; n = 3 per genotype).

Spontaneous and induced gamma oscillations are altered in PV-Cre/NR1f/f mice

We have previously described that activation of FS-PV interneurons enhances gamma oscillations in neocortex *in vivo* (4), in agreement with substantial correlative and theoretical prior evidence (34, 35). Somatosensory cortex represents a local circuit with well-described anatomy and function, arguably being the most widely employed model of neocortical function in the rodent. FS-PV interneurons are local circuit neurons, and recent studies in somatosensory cortex have provided substantial progress for our understanding of fast-spiking behavior in gamma rhythm generation in general cortical network functions *in vivo* (4, 6). There is also a substantial prior work measuring receptive fields of FS interneurons in this specific cortical area (36-38). Recently, it was shown that NMDAR antagonists increase the power of basal gamma oscillations in rodents (13). Abnormal gamma was found to be ongoing simultaneously all over the cerebral cortex (prefrontal, frontal, parietal and occipital areas) in free-moving, sedated and anesthetized animals (13). The dysfunction in information processing found in schizophrenic patients is not limited to high-order association cortex, such as prefrontal cortex, but also influences sensory cortex (39). To identify potential changes in baseline cortical rhythms, we recorded spontaneous local field potentials (LFP) in layers 2/3 and 4 of primary somatosensory (barrel) cortex of anesthetized PV-Cre/NR1f/f mice (n = 8 sites in 5 control mice and 10 sites in 6 PV-Cre/NR1f/f mice; Figure 2a and b). We found a significant decrease in relative power (27-29) in the 6-10 Hz theta frequency band ($P < 0.05$; Figure 2b) and a significant increase in relative power in the 36-44 Hz gamma frequency band ($P < 0.05$; Figure 2b) in PV-Cre/NR1f/f mice compared to control mice, whereas LFP activity at slightly lower frequencies in the 12-24 Hz beta frequency band was not significantly altered in baseline conditions in PV-Cre/NR1f/f mice (Figure 2b).

Regular spiking (RS), putative excitatory neurons in PV-Cre/NR1f/f mice showed a significantly higher spontaneous firing rate (n = 16 cells; 0.49 ± 0.09 Hz) than did RS cells in control mice (n = 18 cells; 0.25 ± 0.06 Hz; Mann-Whitney test; $P < 0.05$; data not shown).

We next tested the role of NMDAR in FS-PV interneurons for the induction of gamma oscillations in cortical networks by direct recruitment of FS-PV interneurons through the specific expression of the light-activated channel Channelrhodopsin-2 (ChR2), as described previously (4). We drove ChR2 expressing FS-PV cells at a range of frequencies (8 to 200 Hz) in bouts of 3 s of 1 ms light pulses (n = 7 sites in 5 control mice and 12 sites in 6 PV-Cre/NR1f/f mice; Figure 2c-f). Across our sample, FS-PV interneurons in control and PV-Cre/NR1f/f mice were driven with high reliability by light pulses (Figure 2c). Light pulses in the gamma range resulted in significant amplification of relative LFP power at those frequencies in control mice ($P < 0.01$; Figure 2d). Driving FS-PV interneurons lacking NMDAR revealed a specific disruption in the ability of the local network to induce gamma oscillations, resulting in a significantly reduced gamma activity enhancement compared to control mice (Figure 2d). The specificity of this disruption to the gamma band in PV-Cre/NR1f/f mice was highlighted when FS-PV cells were driven at 8, 24 and 40 Hz, respectively (Figure 2e). The oscillatory disruption was not complete as optogenetic stimulation at 24 or 40 Hz each induced significantly increased activity compared to baseline conditions in PV-Cre/NR1f/f mice ($P < 0.05$; Figure 2f).

We used randomly patterned light stimulation (broadband stimulation (4)) of FS-PV interneurons to probe the emergent properties of the local cortical circuit. This

paradigm, in agreement with periodic light stimulation, evoked a significant increase in 20-30 Hz and 36-44 Hz activity in control ($P < 0.05$) but not PV-Cre/NR1/f/f mice ($P > 0.05$; n = 7 sites in 5 control and 10 sites in 6 PV-Cre/NR1f/f mice; Figure 2g).

To probe the impact of NMDAR deletion on recruitment of FS-PV interneurons, we analyzed spike latency and variance in spike timing following optical stimulation in PV-Cre/NR1f/f mice. We found a diminished spike synchronization of FS units in response to light activation (Supplementary Figure 2b, c, g) compared to control mice (Supplementary Figure 2e-g) with significantly increased spike latency and variance in spike timing. As shown in this example, we observed reduced inhibition of RS neurons early in the gamma cycle (4-10 ms after light pulse; Supplementary Figure 2a, c) as well as diminished entrainment of the RS neurons at the end of the cycle (around 20 ms after light pulse; Supplementary Figure 2a, c) compared to control mice (Supplementary Figure 2d, f).

Computational modeling, described below, suggests that reduced synchronization of the FS-PV population results in higher gamma band activity during baseline conditions as well as a reduced ability to recruit and synchronize the local network during higher levels of excitatory activity (Supplementary Figure 3a).

To test whether deficits in cortical network activity were also present in awake behaving animals, we performed LFP recordings in layers 2/3 and 4 of somatosensory cortex in freely moving PV-Cre/NR1f/f (n = 7) or control mice (n = 7) during behavior in a novel environment. We observed prominent gamma-band oscillations in both genotypes (Figure 3a). During a baseline recording period, PV-Cre/NR1f/f mice exhibited a non-significant trend towards elevated spontaneous LFP in the 30-80 Hz gamma range

independent of specific behaviors such as grooming or active exploration, compared to control mice (Figure 3b). PV-Cre/NR1f/f mice showed significantly longer mean event durations for spontaneous gamma oscillations compared to control mice ($P < 0.005$) without changes in the number of gamma events (Figure 3c).

To explore the role of NMDAR in PV interneurons on evoked gamma activity in the awake state, we challenged PV-Cre/NR1f/f mice with an acute administration of the non-competitive NMDAR antagonist MK-801 (0.5 mg/kg; IP; Figure 3d-g) or saline (data not shown). In agreement with previous findings[14], control mice acutely displayed a significant increase in LFP in the 30-50 Hz gamma range (Post1, 5-15 min after MK-801 administration; $P < 0.05$, Wilcoxon signed-rank test; Figure 3e). PV-Cre/NR1f/f mice, in contrast, displayed a significant reduction in gamma-band activity after NMDAR antagonist treatment (Figure 3e). Control mice and PV-Cre/NR1f/f mice displayed a significant induction in the 6-10 Hz frequency band relative power at later time points (Post2, 25-35 min after MK-801 administration; Supplementary Figure 4a and b). In the 12-24 Hz band, the relative power remained unchanged in control animals during the same time frame, but was significantly reduced in PV-Cre/NR1f/f animals (Supplementary Figure 4c and d). Saline treatment did not induce any significant changes in locomotor behavior or relative power in any frequency band between genotypes throughout the duration of the recording sessions (data not shown).

To interpret the findings relative to established theories of gamma emergence, we conducted simulations using a modified form of an established neural circuit model (40). We simulated NMDAR dysfunction in FS-PV interneurons and found emergence of higher frequency oscillations in baseline activity, analogous to the experimental data

(Supplementary Figure 3a and Supplementary Text; Modeling results). We also observed a significant reduction in gamma-band activity following simulation of pharmacological NMDAR inhibition in a PV-Cre/NR1f/f network (Supplementary Figure 3b and Supplementary Text; Modeling results). In addition, we found an increase in the latency and variation of the FS-PV response to simulated light drive that may be responsible for the smaller enhancement of gamma power in this condition (Supplementary Figure 3c and Supplementary Text; Modeling results).

Behavioral effects of NMDAR deletion in parvalbumin cells

We characterized the PV-Cre/NR1f/f mice in a series of paradigms to assess general locomotor and exploratory behaviors as well as cognitive tasks evaluating learning and memory. The PV-Cre/NR1f/f mice and their littermate controls (NR1f/f) were introduced into an automated novel open field environment at an age of 7 weeks (n = 11 per genotype). We did not observe any consistent behavioral differences between PV-Cre/NR1f/f and control mice over the entire 60 min trial or in any 5 min block after analysis of 18 different parameters, including total distance (Figure 4a), locomotion, stereotypy and center/margin time (data not shown).

We questioned whether PV-Cre/NR1f/f mice at later stages develop behavioral abnormalities in the open field and therefore assessed mice of 11-12 weeks of age (n = 9 per genotype). We found a non-significant trend towards a decrease in total distance traveled over the 60 min period for PV-Cre/NR1f/f mice compared to control mice ($P > 0.05$; Mann-Whitney test; Figure 4b). Analysis of time spent in the center (Figure 4c) or

margin of the open field, vertical movements (data not shown) or stereotypy counts (Figure 4d) did not reveal differences between the genotypes over the 60 min period.

Our electrophysiological findings indicate that the PV-Cre/NR1f/f mice have a selective deficit in gamma emergence following optogenetic drive of FS-PV interneurons or pharmacological NMDAR inhibition. To investigate potential behavioral differences in response to acute NMDAR inhibition, we exposed naïve PV-Cre/NR1f/f and control mice (n = 11 per genotype) to the open field for 30 min and then challenged them with administration of the NMDAR antagonist MK-801 at a low dose (0.3 mg/kg) followed by continued exposure to the open field for 60 min. Control mice responded over time to MK-801 administration with increased horizontal activity and induction of stereotypies as previously reported (31) (Figure 4e and f). In contrast, PV-Cre/NR1f/f mice showed a markedly reduced sensitivity to MK801 (Figure 4e and f), consistent with our electrophysiological findings that PV interneurons are an important target for the non-competitive NMDAR antagonists.

Prepulse inhibition (PPI) is associated with deficiencies in sensory information filtering and has been well characterized in schizophrenia (41, 42). PPI deficits have repetitively been found in schizophrenia patients and their unaffected first-degree relatives. Interneurons are considered to be of important for phase-dependent inhibition and circuit oscillations that in turn regulate information processing. Our evaluation of PPI in PV-Cre/NR1f/f mice compared to control mice did not reveal any significant changes in PPI over several prepulse intensities (70-90 dB) (Figure 5a, n = 17 control mice, 15 PV-Cre/NR1f/f mice). Importantly, the startle response was not different between control

mice and PV-Cre/NR1f/f mice (Supplementary Figure 5a and b), thereby excluding sensorimotor defects.

Loss of NMDAR in PV cells results in selective cognitive disruptions

Several studies have analyzed the role of NMDAR in pyramidal neurons during learning and memory by pharmacological NMDAR inhibition (43) or with genetic approaches (23, 44). The contribution of interneurons to learning and memory processes has been proposed (45) but not genetically evaluated, and interneurons display similar NMDAR-dependent electrophysiological properties as pyramidal neurons (46). Habituation is considered to be one of the simplest forms of learning and is disrupted by NMDAR antagonists (41, 47). Accordingly, we observed a significant reduction in acoustic startle habituation in PV-Cre/NR1f/f mice, supporting the NMDAR-dependent contribution of PV interneurons to learning and memory (Figure 5b and Supplementary Figure 5c).

To investigate the role of NMDAR in PV cells for associative learning processes, we exposed mice to cued and contextual fear conditioning paradigms (n = 5 per genotype). Mice were exposed to a neutral conditioned stimulus (sound) in a novel environment paired with an aversive foot shock as the unconditioned stimulus. PV-Cre/NR1f/f mice exhibited impaired associative learning both in a tone-dependent trial 24 h later ($P < 0.05$, Mann-Whitney test; Figure 5c) and a contextual version of the test ($P < 0.05$, Mann-Whitney test; Figure 5d).

To evaluate spatial reference memory, we used a water maze task with a fixed hidden platform consisting of two trials per day with a 5 min intratrial interval. Infusion

of NMDAR antagonists has revealed a critical role for NMDAR during learning and memory for spatial reference memory (43), although the specific contribution of NMDAR on interneurons has not been addressed. The rate of learning in the water maze task over 8 days was not impaired in PV-Cre/NR1f/f mice compared to controls (Figure 5e; escape latency, $P = 0.8794$, two-way analysis of variance (ANOVA); n = 8 control and 11 PV-Cre/NR1f/f mice). The probe trial on day 9 did not reveal significant differences in target quadrant preference compared with control mice ($P = 0.33$ for target quadrant, unpaired t-test; Figure 5f). To address potential impairments in reversal learning, we introduced the hidden platform in a different quadrant and continued the learning paradigm for 4 days. Learning rates for the new platform location over 4 days were not significantly different between genotypes ($P = 0.513$, two-way ANOVA) and a probe trial on the 5th day did not reveal target quadrant preference differences between genotypes ($P = 0.9$ for target quadrant, unpaired t-test; Figure 5g).

Working memory deficits in schizophrenic patients (48-50), and computational models implicate NMDAR as a critical component of working memory (51), with inhibition being important in shaping the time-dependent firing of pyramidal cells in neocortical circuits during cognitive tasks (52). Further, NMDAR antagonists disrupt working memory in humans (53) and rodents (54). We assessed working memory in a T-maze (the discrete paired-trial variable-delay T-maze task (30); n = 10 control and 9 PV-Cre/NR1f/f mice). Both genotypes behaved similarly during the 10 days of training (Supplementary Figure 5d). After training, we performed 10 trials per mouse each day with varying intratrial intervals, to evaluate effects of working memory load on performance. The PV-Cre/NR1f/f mice performed similarly to control mice at 20 s and

40 s intratrial intervals (Figure 5h). In contrast, the 1 s intratrial interval revealed a marked difference between genotypes, with PV-Cre/NR1f/f mice remaining at 65 % accuracy whereas control mice were significantly better with 82 % accuracy ($P < 0.01$; Figure 5h). PV-Cre/NR1f/f mice therefore performed at similar accuracy levels independent of working memory load.

Discussion

We have investigated the *in vivo* function of NMDAR specifically in FS-PV interneurons in regulating cortical brain rhythms and cognitive functions (Supplementary Table 1). This work is based on a long-standing hypothesis connecting PV interneuron dysfunction, NMDAR hypofunction and disturbances in brain rhythms associated with cognitive tasks/functions. We find that NMDAR signaling in FS-PV interneurons is critical for the regulation of gamma oscillations during baseline conditions as well as for gamma rhythm induction. The data we present on optogenetic drive in the superficial cortical layers is specific to FS-PV interneurons, as PV expressing cells in these laminae are only FS interneurons. That said, PV expressing neurons are present throughout the brain. One alternative cell type that could impact our findings is PV expressing thalamic neurons, which typically project to the granular layers in cortex. There is correlative (neurophysiological), causal (optogenetic) and computational (modeling) evidence that neocortical gamma oscillations depend crucially on local FS interneurons, but these studies also suggest that the tonic level of excitation to the neocortical circuit is key. As such, alternations in these thalamic neurons could have impacted, for example, our baseline data.

The inability of the cortical network to induce additional gamma oscillations by direct activation of FS-PV interneurons might indicate an impairment of network flexibility. The results suggest that PV-Cre/NR1f/f mice exhibit spontaneous and evoked network abnormalities similar to those observed after low does administration of NMDAR antagonists (13). This is similar to findings in psychiatric patients, who display aberrant recruitment of cortical circuits and diminished evoked gamma rhythm in response to cognitive and sensory tasks (55). The reduced gamma-band activity after NMDAR antagonist treatment in PV-Cre/NR1f/f mice supports the hypothesis that FS-PV interneurons are an important target for pharmacological NMDAR blockade associated with altered gamma rhythms (13, 56), consistent with our computational model of the PV-Cre/NR1f/f cortical circuit.

We have further found a dissociation between the requirement for NMDAR in FS-PV interneurons during baseline behavior versus demanding cognitive tasks. While the small age-dependent effects in the open field may be of interest in light of behavioral changes associated with transitions from adolescence to adulthood, our results suggest a subtle behavioral effect at most of NMDAR deficiency in PV interneuron in the unchallenged state. This finding is in contrast to the phenotypes of hyperlocomotion and stereotypical behaviors in mice with general NMDAR hypofunction (31, 32).

Working memory includes executive components such as goal maintenance and interference control (57). It is difficult to establish the explicit role of executive components in rodent working memory tasks, and in addition, several cognitive processes and memory systems may be used in conjunction in the tasks (57). While the selective working memory deficit in performance of the PV-Cre/NR1f/f mice at short delays in the

discrete paired-trial variable-delay T-maze task most likely represent a complex network deficit, these data suggest that activation of NMDAR on PV interneurons is required for rapid initiation of the working memory encoding phase. In contrast, PV-Cre/NR1f/f mice displayed intact spatial reference memory, as measured in the Morris water maze task. In line with this, mice with deletion of the α-amino-3-hydroxy-5-methyl-4-isoxazolepropionic acid (AMPA) receptor GluR-A specifically in PV expressing interneurons (58) do not show impaired spatial reference memory, but have reduced kainate-induced gamma oscillations in hippocampal slices. Our results point to a specific role for NMDAR in PV interneurons in memory tasks involving the neocortex, amygdala and hippocampus. A potential unifying feature of these forms of memory is their dependence on intact gamma rhythms, which are enhanced during exposure to novel environments (59), but might play a lesser role in long-term learning in the water-maze task or the longer intratrial intervals in the T-maze task.

Evidence supporting the important role of NMDAR in interneurons has recently been provided through genetic deletion of NMDAR in a mixed population of GABAergic interneurons, including PV interneurons (60). This deletion results in a wide range of behavioral phenotypes, including novelty-induced hyperlocomotion, PPI deficits and anxiety-like effects, which were not observed in PV-Cre/NR1f/f mice. Our model of a targeted adolescent disruption of NMDAR transmission specifically in PV interneurons, provides a specific framework for understanding the role of NMDA transmission in PV interneurons for oscillatory activities in neuronal ensembles.

An important question is to what extent the observed circuit deficits depend on specific NMDAR related activities, or represent a general hypoexcitability of PV

interneurons conferred by diminished glutamatergic drive. It has been shown that reduced excitatory recruitment of PV interneurons through loss of AMPA receptors affects ongoing and induced gamma oscillations in hippocampal slices (58), with corresponding deficits in working memory but not spatial reference memory. Our *in vivo* physiological, behavioral studies, and computational modeling suggest that such deficits, found in our mouse model as well, could reflect a general decrease in excitability of PV interneurons.

There is direct evidence for NMDAR hypofunction in psychiatric patients (61). Additionally, human genetic data for schizophrenia-associated genes have implicated the NMDAR signaling pathway and disruption of the Neuregulin-1/ErbB4 pathway (62-64). PV interneurons express ErbB4 protein (65) and the Neuregulin-1/ErbB4 pathway plays a role in gamma oscillations (66). However, we emphasize that the PV-Cre/NR1f/f mouse does not represent a model of schizophrenia, but rather contributes to the investigation of possibly one dimension of schizophrenia that includes cognitive defects. Further, under even the best circumstances, a mouse model is limited in its ability to recapitulate all complex cognitive dimensions that have evolved in humans.

Acknowledgements

The authors would like to thank for valuable advice on behavioral assays from Tracey Petryshen, Erin Berry, Mike Lewis, Nadine Joseph and Ji-Song Guan. M.C is supported by a NARSAD Young Investigator Award. M.C and K. M. are supported by Knut and Alice Wallenbergs Foundation.

Conflict of interest

The authors declare no conflict of interest.

References

1. Jones RS, Buhl EH. Basket-like interneurones in layer II of the entorhinal cortex exhibit a powerful NMDA-mediated synaptic excitation. *Neurosci Lett* 1993 Jan 4; **149**(1)**:** 35-39.

2. Buzsaki G, Leung LW, Vanderwolf CH. Cellular bases of hippocampal EEG in the behaving rat. *Brain Res* 1983 Oct; **287**(2)**:** 139-171.

3. Traub RD, Whittington MA, Stanford IM, Jefferys JG. A mechanism for generation of long-range synchronous fast oscillations in the cortex. *Nature* 1996 Oct 17; **383**(6601)**:** 621-624.

4. Cardin JA, Carlen M, Meletis K, Knoblich U, Zhang F, Deisseroth K *et al.* Driving fast-spiking cells induces gamma rhythm and controls sensory responses. *Nature* 2009 Jun 4; **459**(7247)**:** 663-667.

5. Fries P. Neuronal gamma-band synchronization as a fundamental process in cortical computation. *Annu Rev Neurosci* 2009; **32:** 209-224.

6. Sohal VS, Zhang F, Yizhar O, Deisseroth K. Parvalbumin neurons and gamma rhythms enhance cortical circuit performance. *Nature* 2009 Jun 4; **459**(7247)**:** 698-702.

7. Uhlhaas PJ, Haenschel C, Nikolic D, Singer W. The role of oscillations and synchrony in cortical networks and their putative relevance for the pathophysiology of schizophrenia. *Schizophr Bull* 2008 Sep; **34**(5)**:** 927-943.

8. Lewis DA, Hashimoto T, Volk DW. Cortical inhibitory neurons and schizophrenia. *Nat Rev Neurosci* 2005 Apr; **6**(4)**:** 312-324.

9. Cunningham MO, Hunt J, Middleton S, LeBeau FE, Gillies MJ, Davies CH *et al.* Region-specific reduction in entorhinal gamma oscillations and parvalbumin-immunoreactive neurons in animal models of psychiatric illness. *J Neurosci* 2006 Mar 8; **26**(10)**:** 2767-2776.

10. Kehrer C, Dugladze T, Maziashvili N, Wojtowicz A, Schmitz D, Heinemann U *et al.* Increased inhibitory input to CA1 pyramidal cells alters hippocampal gamma frequency oscillations in the MK-801 model of acute psychosis. *Neurobiol Dis* 2007 Mar; **25**(3)**:** 545-552.

11. Sagratella S, Pezzola A, Popoli P, Scotti de Carolis AS. Different capability of N-methyl-D-aspartate antagonists to elicit EEG and behavioural phencyclidine-like effects in rats. *Psychopharmacology (Berl)* 1992; **109**(3)**:** 277-282.

12. Ma J, Leung LS. Relation between hippocampal gamma waves and behavioral disturbances induced by phencyclidine and methamphetamine. *Behav Brain Res* 2000 Jun 15; **111**(1-2)**:** 1-11.

13. Hakami T, Jones NC, Tolmacheva EA, Gaudias J, Chaumont J, Salzberg M *et al.* NMDA receptor hypofunction leads to generalized and persistent aberrant gamma oscillations independent of hyperlocomotion and the state of consciousness. *PLoS One* 2009; **4**(8)**:** e6755.

14. Ehrlichman RS, Gandal MJ, Maxwell CR, Lazarewicz MT, Finkel LH, Contreras D *et al.* N-methyl-d-aspartic acid receptor antagonist-induced frequency oscillations in mice recreate pattern of electrophysiological deficits in schizophrenia. *Neuroscience* 2009 Jan 23; **158**(2)**:** 705-712.

15. Pinault D. N-methyl d-aspartate receptor antagonists ketamine and MK-801 induce wake-related aberrant gamma oscillations in the rat neocortex. *Biol Psychiatry* 2008 Apr 15; **63**(8)**:** 730-735.

16. Javitt DC, Zukin SR. Recent advances in the phencyclidine model of schizophrenia. *Am J Psychiatry* 1991 Oct; **148**(10)**:** 1301-1308.

17. Coyle JT, Tsai G, Goff D. Converging evidence of NMDA receptor hypofunction in the pathophysiology of schizophrenia. *Ann N Y Acad Sci* 2003 Nov; **1003:** 318-327.

18. Krystal JH, Anand A, Moghaddam B. Effects of NMDA receptor antagonists: implications for the pathophysiology of schizophrenia. *Arch Gen Psychiatry* 2002 Jul; **59**(7)**:** 663-664.

19. Saykin AJ, Gur RC, Gur RE, Mozley PD, Mozley LH, Resnick SM *et al.* Neuropsychological function in schizophrenia. Selective impairment in memory and learning. *Arch Gen Psychiatry* 1991 Jul; **48**(7)**:** 618-624.

20. Cho RY, Konecky RO, Carter CS. Impairments in frontal cortical gamma synchrony and cognitive control in schizophrenia. *Proc Natl Acad Sci U S A* 2006 Dec 26; **103**(52)**:** 19878-19883.

21. Kwon JS, O'Donnell BF, Wallenstein GV, Greene RW, Hirayasu Y, Nestor PG *et al.* Gamma frequency-range abnormalities to auditory stimulation in schizophrenia. *Arch Gen Psychiatry* 1999 Nov; **56**(11)**:** 1001-1005.

22. Hippenmeyer S, Vrieseling E, Sigrist M, Portmann T, Laengle C, Ladle DR *et al.* A developmental switch in the response of DRG neurons to ETS transcription factor signaling. *PLoS Biol* 2005 May; **3**(5)**:** e159.

23. Tsien JZ, Huerta PT, Tonegawa S. The essential role of hippocampal CA1 NMDA receptor-dependent synaptic plasticity in spatial memory. *Cell* 1996 Dec 27; **87**(7)**:** 1327-1338.

24. Srinivas S, Watanabe T, Lin CS, William CM, Tanabe Y, Jessell TM *et al.* Cre reporter strains produced by targeted insertion of EYFP and ECFP into the ROSA26 locus. *BMC Dev Biol* 2001; **1:** 4.

25. Ryu J, Futai K, Feliu M, Weinberg R, Sheng M. Constitutively active Rap2 transgenic mice display fewer dendritic spines, reduced extracellular signal-regulated kinase signaling, enhanced long-term depression, and impaired spatial learning and fear extinction. *J Neurosci* 2008 Aug 13; **28**(33)**:** 8178-8188.

26. Hung AY, Futai K, Sala C, Valtschanoff JG, Ryu J, Woodworth MA *et al.* Smaller dendritic spines, weaker synaptic transmission, but enhanced spatial learning in mice lacking Shank1. *J Neurosci* 2008 Feb 13; **28**(7)**:** 1697-1708.

27. Gasser T, Bacher P, Mocks J. Transformations towards the normal distribution of broad band spectral parameters of the EEG. *Electroencephalogr Clin Neurophysiol* 1982 Jan; **53**(1)**:** 119-124.

28. Cardin JA, Palmer LA, Contreras D. Stimulus-dependent gamma (30-50 Hz) oscillations in simple and complex fast rhythmic bursting cells in primary visual cortex. *J Neurosci* 2005 Jun 1; **25**(22)**:** 5339-5350.

29. Joho RH, Ho CS, Marks GA. Increased gamma- and decreased delta-oscillations in a mouse deficient for a potassium channel expressed in fast-spiking interneurons. *J Neurophysiol* 1999 Oct; **82**(4)**:** 1855-1864.

30. Aultman JM, Moghaddam B. Distinct contributions of glutamate and dopamine receptors to temporal aspects of rodent working memory using a clinically relevant task. *Psychopharmacology (Berl)* 2001 Jan; **153**(3)**:** 353-364.

31. Mohn AR, Gainetdinov RR, Caron MG, Koller BH. Mice with reduced NMDA receptor expression display behaviors related to schizophrenia. *Cell* 1999 Aug 20; **98**(4)**:** 427-436.

32. Labrie V, Lipina T, Roder JC. Mice with reduced NMDA receptor glycine affinity model some of the negative and cognitive symptoms of schizophrenia. *Psychopharmacology (Berl)* 2008 Oct; **200**(2)**:** 217-230.

33. del Rio JA, de Lecea L, Ferrer I, Soriano E. The development of parvalbumin-immunoreactivity in the neocortex of the mouse. *Brain Res Dev Brain Res* 1994 Sep 16; **81**(2)**:** 247-259.

34. Fries P, Nikolic D, Singer W. The gamma cycle. *Trends Neurosci* 2007 Jul; **30**(7)**:** 309-316.

35. Bartos M, Vida I, Jonas P. Synaptic mechanisms of synchronized gamma oscillations in inhibitory interneuron networks. *Nat Rev Neurosci* 2007 Jan; **8**(1)**:** 45-56.

36. Andermann ML, Ritt J, Neimark MA, Moore CI. Neural correlates of vibrissa resonance; band-pass and somatotopic representation of high-frequency stimuli. *Neuron* 2004 May 13; **42**(3)**:** 451-463.

37. Swadlow HA. Efferent neurons and suspected interneurons in S-1 vibrissa cortex of the awake rabbit: receptive fields and axonal properties. *J Neurophysiol* 1989 Jul; **62**(1)**:** 288-308.

38. Andermann ML, Moore CI. A somatotopic map of vibrissa motion direction within a barrel column. *Nat Neurosci* 2006 Apr; **9**(4)**:** 543-551.

39. Javitt DC, Doneshka P, Zylberman I, Ritter W, Vaughan HG, Jr. Impairment of early cortical processing in schizophrenia: an event-related potential confirmation study. *Biol Psychiatry* 1993 Apr 1; **33**(7)**:** 513-519.

40. Vierling-Claassen D, Siekmeier P, Stufflebeam S, Kopell N. Modeling GABA alterations in schizophrenia: a link between impaired inhibition and altered gamma and beta range auditory entrainment. *J Neurophysiol* 2008 May; **99**(5)**:** 2656-2671.

41. Braff DL, Geyer MA. Sensorimotor gating and schizophrenia. Human and animal model studies. *Arch Gen Psychiatry* 1990 Feb; **47**(2)**:** 181-188.

42. Turetsky BI, Calkins ME, Light GA, Olincy A, Radant AD, Swerdlow NR. Neurophysiological endophenotypes of schizophrenia: the viability of selected candidate measures. *Schizophr Bull* 2007 Jan; **33**(1)**:** 69-94.

43. Morris RG, Anderson E, Lynch GS, Baudry M. Selective impairment of learning and blockade of long-term potentiation by an N-methyl-D-aspartate receptor antagonist, AP5. *Nature* 1986 Feb 27-Mar 5; **319**(6056)**:** 774-776.

44. Nakazawa K, Quirk MC, Chitwood RA, Watanabe M, Yeckel MF, Sun LD *et al.* Requirement for hippocampal CA3 NMDA receptors in associative memory recall. *Science* 2002 Jul 12; **297**(5579)**:** 211-218.

45. Paulsen O, Moser EI. A model of hippocampal memory encoding and retrieval: GABAergic control of synaptic plasticity. *Trends Neurosci* 1998 Jul; **21**(7)**:** 273-278.

46. Lamsa K, Heeroma JH, Kullmann DM. Hebbian LTP in feed-forward inhibitory interneurons and the temporal fidelity of input discrimination. *Nat Neurosci* 2005 Jul; **8**(7)**:** 916-924.

47. Klamer D, Palsson E, Revesz A, Engel JA, Svensson L. Habituation of acoustic startle is disrupted by psychotomimetic drugs: differential dependence on dopaminergic and nitric oxide modulatory mechanisms. *Psychopharmacology (Berl)* 2004 Nov; **176**(3-4)**:** 440-450.

48. Goldman-Rakic PS. The physiological approach: functional architecture of working memory and disordered cognition in schizophrenia. *Biol Psychiatry* 1999 Sep 1; **46**(5)**:** 650-661.

49. Wexler BE, Stevens AA, Bowers AA, Sernyak MJ, Goldman-Rakic PS. Word and tone working memory deficits in schizophrenia. *Arch Gen Psychiatry* 1998 Dec; **55**(12)**:** 1093-1096.

50. Forbes NF, Carrick LA, McIntosh AM, Lawrie SM. Working memory in schizophrenia: a meta-analysis. *Psychol Med* 2009 Jun; **39**(6)**:** 889-905.

51. Lisman JE, Fellous JM, Wang XJ. A role for NMDA-receptor channels in working memory. *Nat Neurosci* 1998 Aug; **1**(4)**:** 273-275.

52. Constantinidis C, Williams GV, Goldman-Rakic PS. A role for inhibition in shaping the temporal flow of information in prefrontal cortex. *Nat Neurosci* 2002 Feb; **5**(2)**:** 175-180.

53. Krystal JH, Karper LP, Seibyl JP, Freeman GK, Delaney R, Bremner JD *et al.* Subanesthetic effects of the noncompetitive NMDA antagonist, ketamine, in humans. Psychotomimetic, perceptual, cognitive, and neuroendocrine responses. *Arch Gen Psychiatry* 1994 Mar; **51**(3)**:** 199-214.

54. Tonkiss J, Rawlins JN. The competitive NMDA antagonist AP5, but not the non-competitive antagonist MK801, induces a delay-related impairment in spatial working memory in rats. *Exp Brain Res* 1991; **85**(2)**:** 349-358.

55. Basar-Eroglu C, Brand A, Hildebrandt H, Karolina Kedzior K, Mathes B, Schmiedt C. Working memory related gamma oscillations in schizophrenia patients. *Int J Psychophysiol* 2007 Apr; **64**(1)**:** 39-45.

56. Homayoun H, Moghaddam B. NMDA receptor hypofunction produces opposite effects on prefrontal cortex interneurons and pyramidal neurons. *J Neurosci* 2007 Oct 24; **27**(43)**:** 11496-11500.

57. Arguello PA, Gogos JA. Cognition in mouse models of schizophrenia susceptibility genes. *Schizophr Bull* Mar; **36**(2)**:** 289-300.

58. Fuchs EC, Zivkovic AR, Cunningham MO, Middleton S, Lebeau FE, Bannerman DM *et al.* Recruitment of parvalbumin-positive interneurons determines hippocampal function and associated behavior. *Neuron* 2007 Feb 15; **53**(4)**:** 591-604.

59. Nitz D, McNaughton B. Differential modulation of CA1 and dentate gyrus interneurons during exploration of novel environments. *J Neurophysiol* 2004 Feb; **91**(2)**:** 863-872.

60. Belforte JE, Zsiros V, Sklar ER, Jiang Z, Yu G, Li Y *et al.* Postnatal NMDA receptor ablation in corticolimbic interneurons confers schizophrenia-like phenotypes. *Nat Neurosci* Jan; **13**(1)**:** 76-83.

61. Pilowsky LS, Bressan RA, Stone JM, Erlandsson K, Mulligan RS, Krystal JH *et al.* First in vivo evidence of an NMDA receptor deficit in medication-free schizophrenic patients. *Mol Psychiatry* 2006 Feb; **11**(2)**:** 118-119.

62. Stefansson H, Sigurdsson E, Steinthorsdottir V, Bjornsdottir S, Sigmundsson T, Ghosh S *et al.* Neuregulin 1 and susceptibility to schizophrenia. *Am J Hum Genet* 2002 Oct; **71**(4)**:** 877-892.

63. Hahn CG, Wang HY, Cho DS, Talbot K, Gur RE, Berrettini WH *et al.* Altered neuregulin 1-erbB4 signaling contributes to NMDA receptor hypofunction in schizophrenia. *Nat Med* 2006 Jul; **12**(7)**:** 824-828.

64. Lau CG, Zukin RS. NMDA receptor trafficking in synaptic plasticity and neuropsychiatric disorders. *Nat Rev Neurosci* 2007 Jun; **8**(6)**:** 413-426.

65. Neddens J, Buonanno A. Selective populations of hippocampal interneurons express ErbB4 and their number and distribution is altered in ErbB4 knockout mice. *Hippocampus* 2009 Aug 4.

66. Fisahn A, Neddens J, Yan L, Buonanno A. Neuregulin-1 modulates hippocampal gamma oscillations: implications for schizophrenia. *Cereb Cortex* 2009 Mar; **19**(3)**:** 612-618.

FIGURE LEGENDS

Figure 1. Genetic ablation of NMDAR specifically in parvalbumin interneurons. a, Quantification of recombination from the parvalbumin locus in somatosensory cortex and hippocampus at different time points. **b, c**, NMDAR-mediated synaptic transmission in parvalbumin interneurons is abolished in PV-Cre/NR1f/f mice. **b**, Sample EPSC traces mediated by the AMPAR (downward) and NMDAR (upward) from a control PV-Cre mouse and a PV-Cre/NR1f/f mouse. **c**, NMDAR EPSC/AMPAR EPSC ratio in control PV-Cre and PV-Cre/NR1f/f mice. **d**, Distribution of parvalbumin interneurons in NR1f/f and PV-Cre/NR1f/f mice, respectively, at 11 w. **e**, Immunohistochemistry for parvalbumin interneurons in somatosensory cortex of an adult NR1f/f and PV-Cre/NR1f/f mouse, respectively. $*P < 0.05$; error bars, mean ± s.e.m. Scale bar: **e**, 200 μm. See also Supplementary Figure 1.

Figure 2. Spontaneous and induced cortical gamma oscillations require NMDAR in parvalbumin interneurons. a, b, d-g, LFP activity in anesthetized control (black bars) and PV-Cre/NR1f/f (red bars) mice. **a**, **b** Spontaneous LFP activity. **a**, Relative power from 1-100 Hz in control and PV-Cre/NR1f/f mice. **b**, Relative LFP power in the 6-10, 12-24 and 36-44 Hz frequency bands. **c**, Single-unit recordings during optogenetic activation of FS-PV+ interneurons. Middle trace: control mice, lower trace: PV-Cre/NR1f/f mice. In each case, a series of 1 ms light pulses (blue trace) was given in a random pattern drawn from a broadband distribution (5-200 Hz). In both cases, each light pulse evoked a single spike from the cell. Both cells followed the light stimulus with a high degree of reliability. **d-g**, Optogenetic activation of FS-PV+ interneurons in somatosensory cortex in control and PV-Cre/NR1f/f mice. **d**, Mean power ratio in each

LFP frequency band in response to light activation of ChR2 expressing FS-PV+ interneurons at varying frequencies. PV-Cre/NR1f/f mice generate significantly less 30-60 Hz oscillations (gamma) than control mice. **e,** Comparison of the effect of activating FS-PV+ interneurons in the control and PV-Cre/NR1f/f mice at 8, 24, and 40 Hz on relative LFP power in those frequency bands. **f**, Relative LFP power in the 8, 24, and 40 Hz frequency bands in the PV-Cre/NR1f/f mice during spontaneous (solid bars) and light-evoked (striped bars) activity. **g,** Relative power in the 6-10, 15-19, 20-30 and 36-44 Hz frequency bands in response to broadband light stimulation in control and PV-Cre/NR1f/f mice. $*P < 0.05$, $**P < 0.01$; error bars, mean ± s.e.m.

Figure 3. Baseline cortical oscillations and NMDAR antagonist induced gamma rhythms in awake behaving animals. a-g, LFP activity in somatosensory cortex in awake control and PV-Cre/NR1f/f mice. **a**, Examples of single-trial gamma activity from a PV-Cre/NR1f/f and control mouse. Thin lines: LFP filtered between 5-300 Hz; thick lines: LFP filtered in the 30-50 Hz gamma frequency range. **b, c,** Awake baseline activity. **b,** Mean power spectra 1-100 Hz. Lighter regions indicate s.e.m. **c,** Characteristics of 30-50 Hz gamma events. Mean event duration is significantly increased in freely moving PV-Cre/NR1f/f mice, whereas number of events are not. **d-g,** NMDAR antagonist (MK-801) challenge. **d**, **e** Average relative power in the 30-50 Hz gamma frequency band 15 min before administration of MK-801 (dashed line), to 35 min after. Lighter regions indicate s.e.m. Administration of MK-801 gives a significant increase in relative gamma power in control mice and a significant reduction in relative gamma power in PV-Cre/NR1f/f mice. **f,** Average power changes (dB) between Pre and Post1.

Lighter regions indicate s.e.m. **g,** Average power changes (dB) between Pre and Post2. Pre, 5-15 min before MK-801; Post1, 5-15 min after MK-801; Post2, 25-35 min after MK-801. *$P < 0.05$; error bars, mean ± s.e.m. See also Supplementary Figure 3 and 4.

Figure 4. PV-Cre/NR1f/f mice display no behavioral changes in the open field but reduced sensitivity to pharmacological NMDAR treatment. a, Total distance traveled over 60 min in the open field of PV-Cre/NR1f/f and control mice at 7w. **b-d**, Open field behavior over 60 min at 11w. **b,** Total distance traveled over 60 min in the open field of PV-Cre/NR1f/f and control mice at 11w. **c**, No significant difference in the time spent in the center of the field between the genotypes. **d**, PV-Cre/NR1f/f mice do not display stereotypy behavior. **e**, MK-801 treatment induces significant increase in horizontal activity only in control mice. **f**, MK-801 treatment results in marked increase in stereotypy behavior only in control mice. HACT, horizontal activity; STR TIME, stereotypy time; STR CNT, stereotypy count; STR NO, stereotypy numbers; ns $P > 0.05$, **$P < 0.01$, ***$P< 0.001$,****$P < 0.0001$; error bars, mean ± s.e.m.

Figure 5. Loss of NMDAR in PV+ interneurons results in selective cognitive disruptions. a, PV-Cre/NR1f/f mice show no deficiency in sensorimotor gating as measured by PPI. **b,** PV-Cre/NR1f/f display deficiencies in habituation. **c**, **d**, PV-Cre/NR1f/f mice exhibit impaired freezing behavior both to a tone-dependent (cued) and a contextual version of fear conditioning. **e**, PV-Cre/NR1f/f mice perform similarly to control mice during training in a hidden platform version of water maze. **f**, Time spent (%) in each quadrant during the water maze probe trial. There is no significant difference

between the genotypes. **g**, Time spent (%) in each quadrant during the water maze probe trial after reversal training. There is no significant difference between the genotypes. **h**, PV-Cre/NR1f/f mice perform at a similar accuracy levels independent of working memory load in the discrete paired-trial variable-delay T-maze task. PPI, prepulse inhibition; FC, fear conditioning; T, target quadrant; R, right quadrant; O, opposite quadrant; L, left quadrant. *$P < 0.05$, **$P < 0.01$; error bars, mean ± s.e.m. See also Supplementary Figure 5.

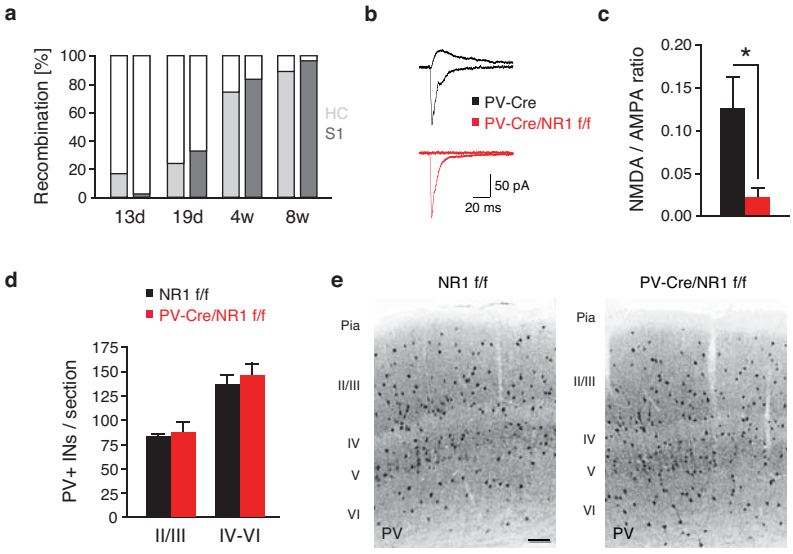
a
Recombination [%]
100
80
60
40
20
0
13d
19d
4w
8w
HC
S1
b
PV-Cre
PV-Cre/NR1 f/f
50 pA
20 ms
c
NMDA / AMPA ratio
0.20
0.15
0.10
0.05
0.00
*
d
NR1 f/f
PV-Cre/NR1 f/f
PV+ INs / section
175
150
125
100
75
50
25
0
II/III
IV-VI
e
NR1 f/f
PV-Cre/NR1 f/f
Pia
II/III
IV
V
VI
PV

Figure 1

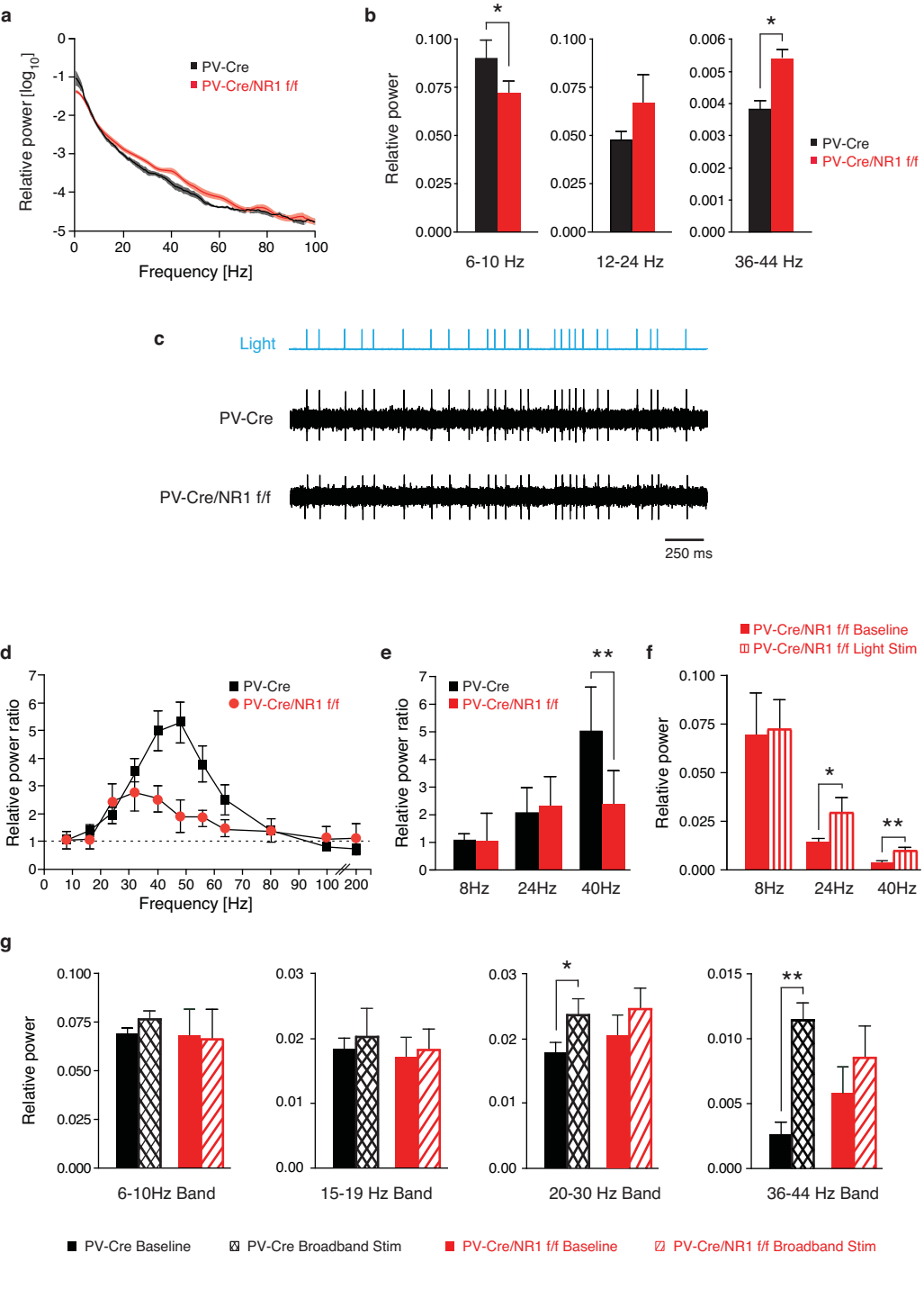
a
Relative power [log10]
Frequency [Hz]
PV-Cre
PV-Cre/NR1 f/f
b
Relative power
6-10 Hz
12-24 Hz
36-44 Hz
PV-Cre
PV-Cre/NR1 f/f
c
Light
PV-Cre
PV-Cre/NR1 f/f
250 ms
d
Relative power ratio
Frequency [Hz]
PV-Cre
PV-Cre/NR1 f/f
e
Relative power ratio
8Hz
24Hz
40Hz
PV-Cre
PV-Cre/NR1 f/f
f
PV-Cre/NR1 f/f Baseline
PV-Cre/NR1 f/f Light Stim
Relative power
8Hz
24Hz
40Hz
g
Relative power
6-10Hz Band
15-19 Hz Band
20-30 Hz Band
36-44 Hz Band
PV-Cre Baseline
PV-Cre Broadband Stim
PV-Cre/NR1 f/f Baseline
PV-Cre/NR1 f/f Broadband Stim

Figure 2

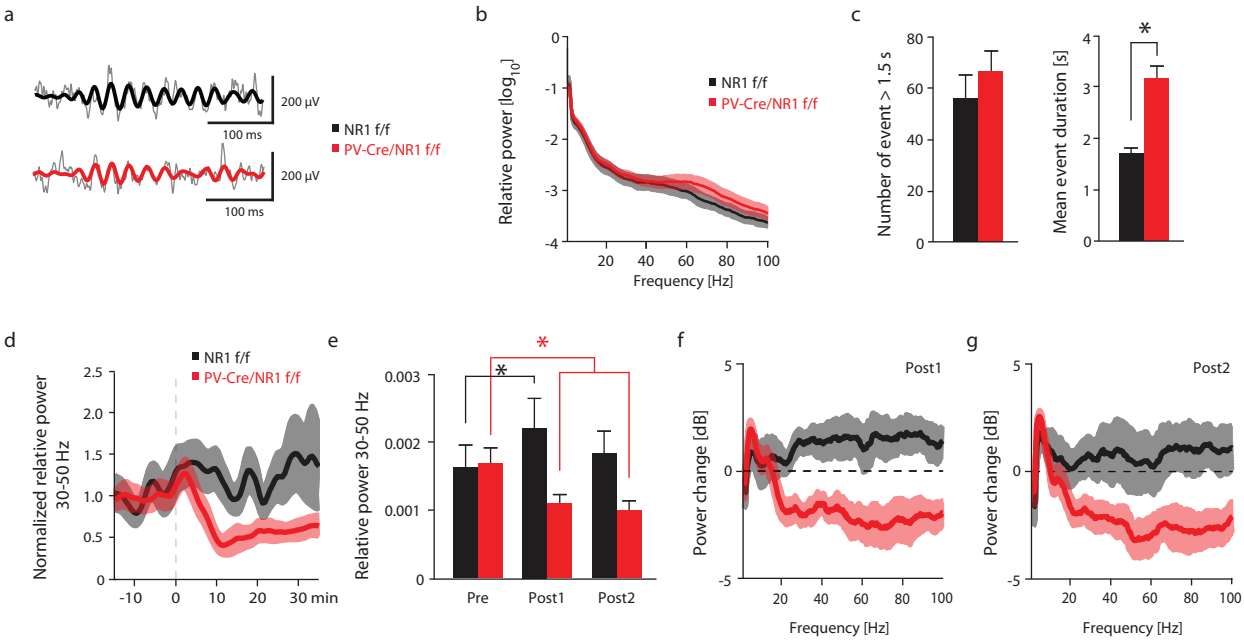
a
200 µV
100 ms
200 µV
100 ms
NR1 f/f
PV-Cre/NR1 f/f
b
Relative power [log10]
Frequency [Hz]
NR1 f/f
PV-Cre/NR1 f/f
c
Number of event > 1.5 s
Mean event duration [s]
*
d
Normalized relative power 30-50 Hz
30 min
NR1 f/f
PV-Cre/NR1 f/f
e
Relative power 30-50 Hz
Pre
Post1
Post2
*
*
f
Post1
Power change [dB]
Frequency [Hz]
g
Post2
Power change [dB]
Frequency [Hz]

Figure 3

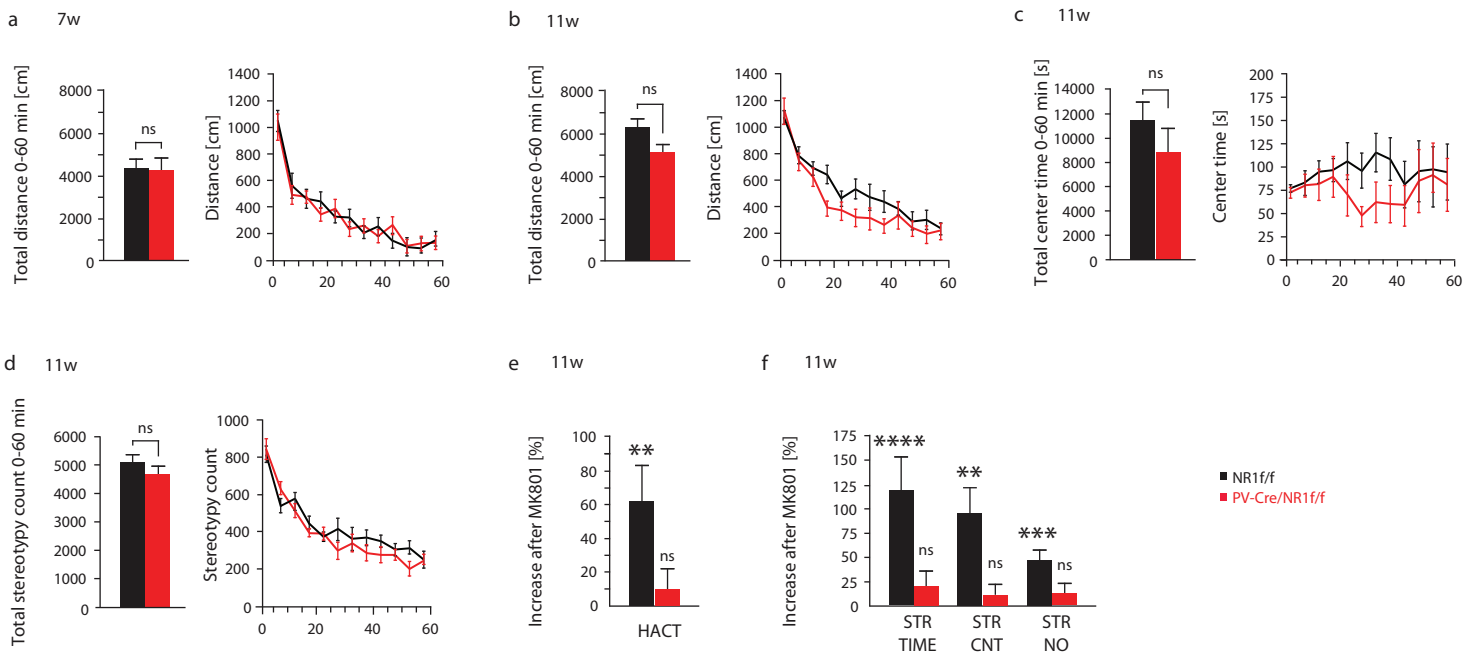
a
7w
Total distance 0-60 min [cm]
ns
Distance [cm]
b
11w
Total distance 0-60 min [cm]
ns
Distance [cm]
c
11w
Total center time 0-60 min [s]
ns
Center time [s]
d
11w
Total stereotypy count 0-60 min
ns
Stereotypy count
e
11w
Increase after MK801 [%]
**
ns
HACT
f
11w
Increase after MK801 [%]
****
**
***
ns
STR TIME
STR CNT
STR NO
NR1f/f
PV-Cre/NR1f/f

Figure 4

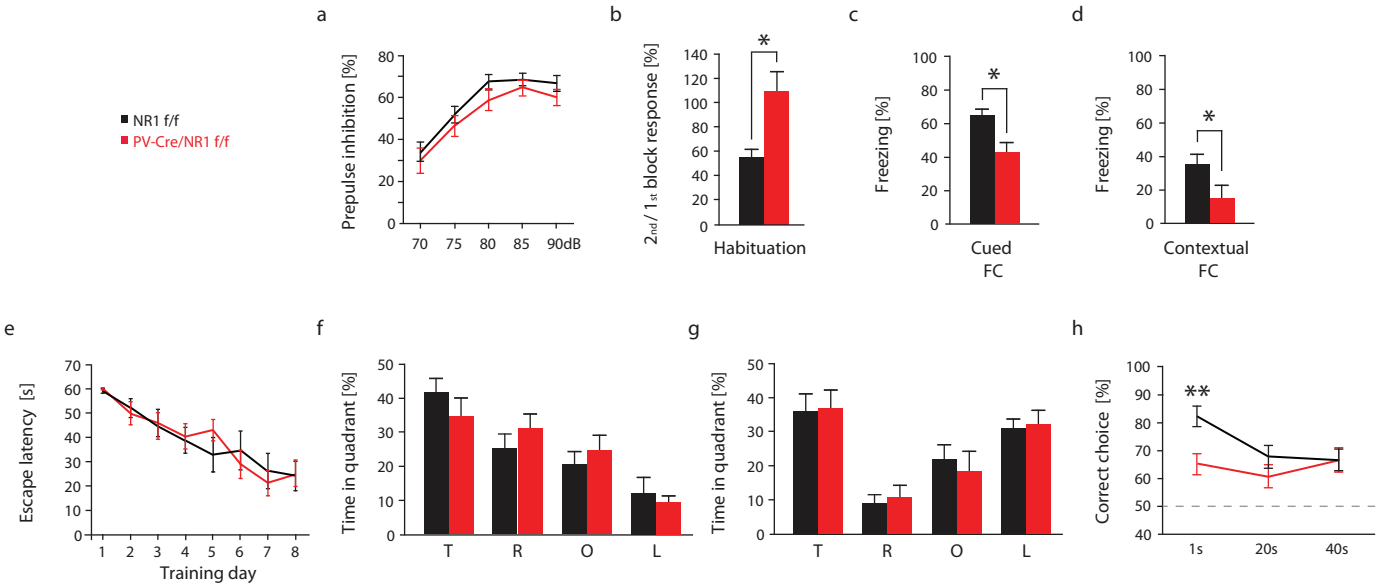
a
b
c
d
NR1 f/f
PV-Cre/NR1 f/f
Prepulse inhibition [%]
70 75 80 85 90dB
2nd / 1st block response [%]
Habituation
Freezing [%]
Cued FC
Contextual FC
e
f
g
h
Escape latency [s]
Training day
Time in quadrant [%]
T R O L
Correct choice [%]
1s 20s 40s

Figure 5